



Product Specifications & Manual

Custom Oligo Synthesis, antisense oligos, RNA oligos, chimeric oligos,
Fluorescent dye labeled oligos, Molecular Beacons, siRNA, phosphonates
Affinity Ligands, 2'-5' linked Oligos

Gold Solid Surface Thiol Oligo Conjugation

Thiol Modifiers, Maleimide, Carboxy I and Amino modifications

For Research Use Only. Not for use in diagnostic procedures for clinical purposes



Gold Solid Surface Thiol Oligonucleotide Conjugation

Introduction to Conjugation or Surface Attachment

Incorporation of reactive organic functional groups, particularly primary amine, thiol (sulfhydryl), or carboxylate groups, at specific sites within an oligonucleotide allows for subsequent conjugation of the oligo with a number of different affinity, reporter or protein labels, depending on the application. Such labels need to be appropriately reactive to the incorporated functional group, for example, N-hydroxy succinimidyl esters (NHS esters, SE) or isothiocyanates in the case of primary amines, and iodoacetamides or maleimides in the case of primary thiols. Examples of labels includes fluorescent dyes/quenchers, digoxigenin, biotin, and enzymes. Functionally-derivitized oligos can also be covalently attached to surfaces such as glass slides or gold microspheres for use in various microarray or nanoelectronic applications.

Conjugation or Surface Attachment Applications

One of the most common applications for amino-modified oligos is for conjugation to fluorescent dyes through an NHS ester. Many dyes with desirable properties (for example, absorption/emission wavelengths or high fluorescence intensity) are not available as phosphoramidites, but only as NHS esters. Rhodamine-based dyes and Alexa dyes are two common examples. Certain haptens such as digoxigenin also require conjugation to amino-labeled oligos via an NHS ester, due to lack of a phosphoramidite for it. Amino-labeled oligos also widely used in the manufacture of DNA microarrays used in gene expression studies, with the oligos covalently immobilized to a glass or other silicon-based flat surface through the amine (1). Thiol-modified oligos can be conjugated to a variety of fluorescent or non-fluorescent molecules; the conjugation chemistry here is typically either maleimide or iodoacetamide-based (2). The orthogonality of the corresponding conjugation chemistries for amine and thiol groups allows for the synthesis of oligos with novel combinations of modifications. Thiol-modified oligos can also be immobilized to glass slides, gold flat surfaces or microspheres for use in DNA microarray, nanoelectronic and DNA sensor-based applications (3, 4). However, because the chemical linkage between a single thiol group and gold is somewhat labile, the DTPA (dithiolphosphoramidite) modification permits multiple tethering of an oligo to a gold surface. Incorporation of three units of DTPA has been shown to provide maximum stability (5).

Conjugation/Surface Attachment--Design Considerations

Over the past 20 years, a wide variety of robust, publicly available protocols have been developed either to conjugate oligonucleotides to chemical moieties (e.g., to haptens, enzymes, fluorescent dyes) for use as probes, or to covalently attach oligonucleotides to a solid surface (e.g., glass slides) for use in DNA microarray applications. Many oligonucleotide-based assays actually combine both of these aspects in one package. Optimal design of such combination assays requires consideration of several different parameters.

I. DNA Microarrays (2-D)

DNA microarrays are excellent platforms for high-density screening applications, as a large number of different sequences can be immobilized to a planar surface for interrogation of a sample. Either amino- or thiol-end-modified oligonucleotides can be covalently attached to glass slides or silicon wafers that have been suitably modified chemically for that purpose. In addition, it is critical that the microarray be designed so that it has the appropriate oligo surface density to ensure sufficient hybridization between immobilized oligo probe and target occurs to

obtain a good signal. In particular, optimal surface coverage decreases with increasing oligo length dependent, presumably due to steric hindrance (6).

II. Microspheres (3-D)

Oligonucleotides attached to microspheres are used in a variety of assays requiring oligos that are immobilized on a solid support that can be freely suspended in solution. The use of magnetic microspheres with oligo-dT to capture mRNA from cell lysates is one well-known application. Another particularly interesting such application is termed “liquid assays”. Here a probe oligo is covalently attached to a polystyrene microsphere containing a fluorescent dye inside them. By using microspheres with different dyes, or dye combinations, and a unique oligo probe for each color microsphere, highly multiplexed, solution-based hybridization assays can be designed in convenient, microtiter-plate format. Such assays exhibit rapid hybridization times, which is an important advantage. It is important to remember, however, that careful optimization of hybridization conditions may need to be done to ensure robust, reproducible detection of all the sample targets being probed for. The targets may be an oligo, cDNA, PCR product, or even a protein, and are fluorescently labeled (with the label different from that of the fluorescent microsphere). After hybridization, the microspheres are typically assayed by flow cytometry, with the fluorescence of the microsphere identifying the probe and the simultaneous fluorescence of the target indicating hybridization (7,8).

III. Conjugation to Amino Modified Oligos

While many chemical moieties are available as phosphoramidites, and so can be directly incorporated into an oligo during synthesis, others are not. The latter often have properties that are particularly useful for oligos slated for use as probes. For example, Alexa dyes (highly fluorescent) and digoxigenin (DIG--low background/high sensitivity in situ probes) are available only as NHS esters. Their incorporation into an oligonucleotide requires the presence of an primary amino group on the oligo for conjugation.

Generally speaking, conjugating an NHS-ester to an amine-modified oligo is an excellent way to generate a modified oligo. The resulting amide linkage between the modification and the oligo is very stable, and the modified oligo can be stored long term at -20°C.

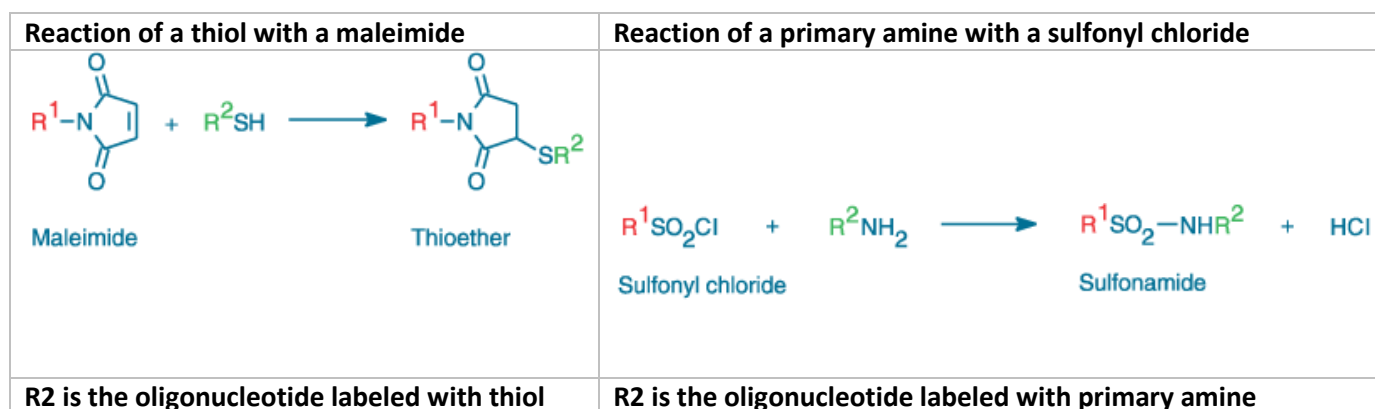
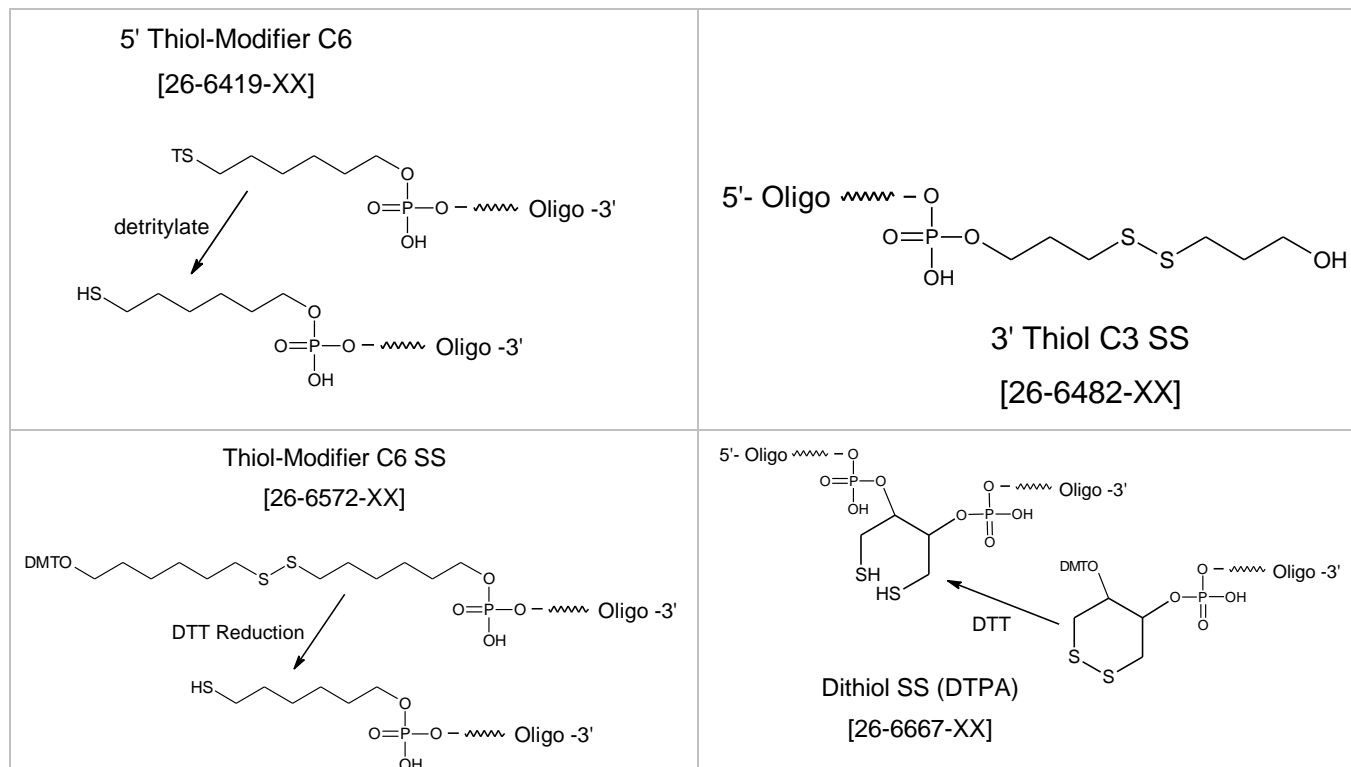
IV. Conjugation to Thiol Modified Oligos

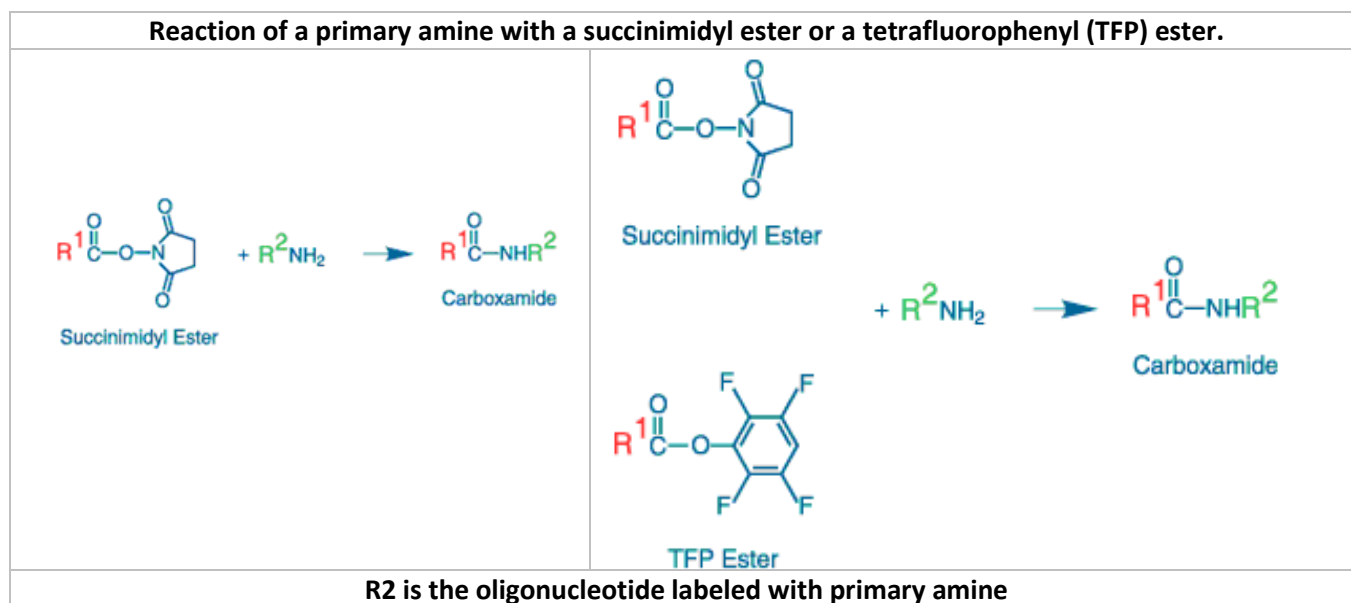
Thiol Modifiers are designed for use in DNA synthesizers to functionalize the custom synthesized target oligonucleotide. The disulfide thiol modifier may be used for introducing 3' - or 5'-thiol linkages. Dithiol Phosphoramidite (DTPA) is a disulfide-containing modifier designed to functionalize synthetic DNA or RNA with multiple thiol groups and can be incorporated at any position of the oligonucleotide. Each DTPA addition leads to two thiol groups. DTPA can be used for multiple reactions with maleimides and other thiol-specific derivatives.

Other modifiers used for conjugation are amino and carboxyl. Amino-Modifiers are available with a variety of chain lengths to fit exactly the desired application. 5'-Carboxy-Modifier C10 is a unique linker designed to be added at the terminus of an oligonucleotide synthesis. It generates an activated carboxylic acid N-hydroxysuccinimide (NHS) ester suitable for immediate conjugation on the synthesis column with molecules containing a primary amine, resulting in a stable amide linkage. PC Amino-Modifier is a photocleavable C6 amino-modifier, part of our line of photocleavable (PC) modifiers.

For research use only. Not for use in diagnostic procedures for clinical purposes.

All thiol modified oligos are treated with 100 mM DTT in ammonia for deprotection that reduces the thiol functional group. These oligos are lyophilized and supplied to the customer in the reduced state.





References

- (1) Immobilization Chemistry. Immobilization of DNA on Chips II, C. Whittman (Vol. Ed.). Springer-Verlag, Berlin, Heidelberg (2005): 51-53.
- (2) Connolly, B.A., Rider, P. Chemical synthesis of oligonucleotides containing a free sulphhydryl group and subsequent attachment of thiol specific probes. *Nucleic Acids Res.* (1985), 13: 4485-4502.
- (3) Roger, Y-H., Jiang-Baucom, P., Huang, Z-J., Bogdanov, V., Anderson, S., Boyce-Jacino, M.T. Immobilization of oligonucleotides onto a glass support via disulfide bonds: A method for preparation of DNA microarrays. *Anal. Biochem.* (1999), 266: 23-30.
- (4) Ackerson, C.J., Sykes, M.T., Kornberg, R.D. Defined DNA/nanoparticle conjugates. *Proc. Natl. Acad. Sci. USA* (2005), 102: 13383-13385.
- (5) Li, Z., Jin, R., Mirkin, C.A., Letsinger, R.L. Multiple thiol-anchor capped DNA-gold nanoparticle conjugates *Nucleic Acids Res.* (2002), 30: 1558-1562.
- (6) Guo, Z., Guilfoyle, R.A., Thiel, A.J., Wang, R., Smith, L.M. Direct fluorescence analysis of genetic polymorphisms by hybridization with oligonucleotide arrays on glass supports. *Nucleic Acids Res.* (1994), 22: 5456-5465.
- (7) Yang, L., Tran, D.K., Wang, X. BADGE, Beads Array for the Detection of Gene Expression, a high-throughput diagnostic bioassay. *Genome Res.* (2001), 11: 1888-1898.
- (8) Defoort, J.P. Simultaneous detection of multiplex-amplified human immunodeficiency virus type 1 RNA, hepatitis C virus RNA, and hepatitis B virus DNA using a flow cytometer microsphere-based hybridization assay. *J. Clin. Microbiol.* (2000), 39: 131-140.

Thiol Modifications for Attachment of Oligos to Gold Surfaces

(Taken from Glen Research)

There has been a lot of development during recent years directed at the application of miniaturization technologies to molecular biology. The ultimate goal is to perform fast molecular tests on microchips. Such microarrays can be fabricated using a variety of technologies, including printing with fine-pointed pins onto glass slides, photolithography with or without pre-made masks, ink-jet printing, or electrochemistry on a microelectrode. These varying technologies allow the manufacturing of microarrays with hundreds, thousands or even millions of specific sequences on solid surfaces that can be glass, silica or gold layered on plastic supports with an area of only 1–2 cm².^{1,2}

The common factors among all microarrays are:

- (i) Oligonucleotides must be irreversibly attached to the solid surface.
- (ii) Hybridization events must be capable of measurement with high accuracy, sensitivity and selectivity, and, if possible in a quantitative way.

Typically, high-density arrays use fluorescence to detect hybridization and such setups are widely commercially available. But there is another technology progressively emerging, which is electrical biosensor detection.³ Osmetech, for example, received FDA clearance in July 2008 for its Warfarin Sensitivity Test and new eSensor[®] XT-8 platform that uses electrochemical detection and oligos attached to gold surfaces.⁴

In most cases, electrochemical detection implies that oligos are attached on a gold surface. Typically, oligos are attached on a gold surface using thiol groups forming a self-assembled monolayer (SAM).⁵ SAMs are molecular layers formed on a surface when it is immersed in a solution containing molecules that specifically interact with this surface. Although different molecules can be immobilized (silanes, carboxylic acids, pyridines, sulphites and thiols) on different surfaces (gold, silver, platinum, copper, mercury and glass), thiols are the most commonly used especially in conjunction with gold surfaces. The stability and organization of the SAMs depend on the forces of attraction between the immobilized molecules, the interaction between terminal groups and their local environment, and the binding force between the surface and the binding group. Oligonucleotide SAMs can be formed directly on the surface when the oligonucleotides contain a pendant thiol group. Or, attachment can be to reactive and previously formed SAMs via EDC. The direct strategy reduces the number of steps required for immobilization and avoids the EDC reaction. However, the indirect strategy (SAMs + EDC) is an alternative when non-saturated monolayers are desired.^{6,7,8}

This immobilization of nucleic acids onto substrates is complex and crucial to the performance of the microarray since (i) the capture probe has to form a stable bond to the substrate, (ii) the spacing of the capture probes has to allow specific binding of the target, (iii) nonspecific adsorption of the material to be arrayed has to be prevented. Consequently, chemisorption of thiols on gold (electrodes) is a common and simple procedure to immobilize probes on a surface. The gold–sulfur bond with a binding energy of about 30–45 kcal/mol (cf. at least 100–150 kcal/mol for a covalent bond) is relatively weak in order to anchor a biopolymer onto a surface.⁹ As reported, mono-functional thiol-terminated oligonucleotides immobilized

on a surface are slowly lost at temperatures between 60 and 90 °C and in the presence of buffers with high salt concentration¹⁰ and are almost completely displaced from the surface when treated with biological buffer systems containing, e.g., dithiothreitol or mercaptoethanol.^{11,12}

In 2003, Glen Research introduced Dithiol Phosphoramidite (DTPA, 10-1937) as a way to attach more than one thiol residue at the extremity of an oligonucleotide. Considering the success of this product, we have now decided to offer a solid support for the easy introduction of this molecule at the 3'-end of an oligonucleotide. Combining the support and the amidite, it is possible to introduce more than one residue, so multiple dithiol residues, conferring an order of magnitude greater stability to the oligo-gold link, can be easily produced. This has been studied in detail⁹ and is illustrated in Figure 3, below. This support can be used as any other support and is available on 1000Å CPG. As shown in Figure 2, below, by combining this support and the existing phosphoramidite, it is easy to create a dithiol tail at the 3'-end of an oligonucleotide. The bond between DTPA and the gold surface is formed spontaneously without need of prior reduction of the disulfide bond. That is the beauty of this product. However, it is important that the gold surface is very clean. Piranha solutions (FRIZ Biochem) may be used for cleaning gold electrodes.

We are also pleased to provide a product that completes our roster, 3'-Thiol-Modifier C6 S-S CPG. We have offered Thiol-Modifier C6 S-S Phosphoramidite (10-1936) for many years, but we only offered the C3 S-S support. We are now introducing the C6 S-S CPG support, also on 1000Å CPG, for convenient 3'-thiol labelling of oligonucleotides. The structure is shown in Figure 1, below.

Figure 1. Structures of Disulfide Reagents	
$\text{DMTO}(\text{CH}_2)_6\text{-S-S-(CH}_2)_6\text{O}$ $\text{(Pr)}_2\text{N-P-OCH}_2\text{CH}_2\text{CN}$	
Thiol-Modifier C6 S-S	DTPA
Thiol-Modifier C6 S-S CPG	DTPA CPG

Figure 2. Synthesis of Multiple DTPA Units at the 3' Terminus

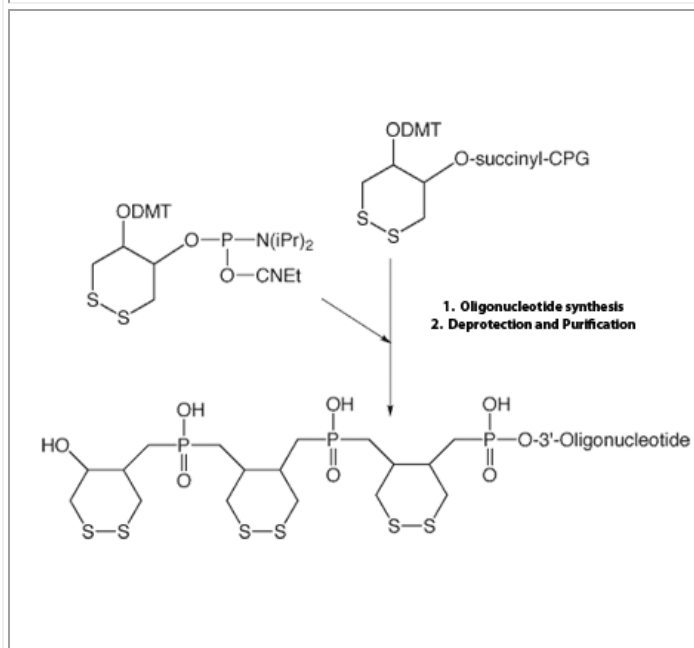
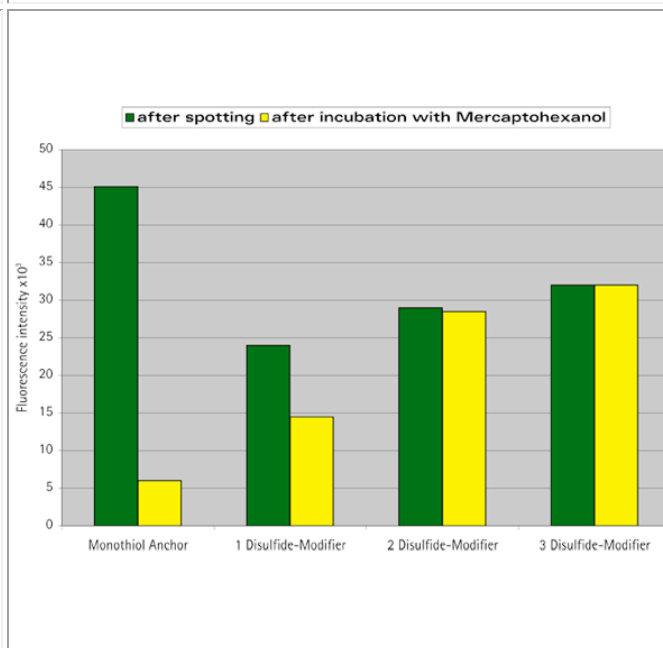


Figure 3. Oligo Fluorescence Intensities



References

1. M.F. Phillips, et al., *Nucleic Acids Res.*, 2008, 36, e7.
2. S.L. Beaucage, *Curr Medicinal Chem*, 2001, 8, 1213-1244.
3. A.A. Gorodetsky, and J.K. Barton, *Langmuir*, 2006, 22, 7917-22.
4. R. Liu, W. Coty, M.W. Reed, and G. Gust, *IVDT*, 2008, 31.
5. R.M. Umek, et al., *J Mol Diagn*, 2001, 3, 74-84.
6. M.R. Lockett, M.F. Phillips, J.L. Jarecki, D. Peelen, and L.M. Smith, *Langmuir*, 2008, 24, 69-75.
7. F. Wei, et al., *Nucleic Acids Res.*, 2008, 36, e65.
8. A.G. Frutos, J.M. Brockman, and R.M. Corn, *Langmuir*, 2000, 16, 2192-2197.
9. P. Liepold, et al., *Anal Bioanal Chem*, 2008, 391, 1759-72.
10. Z. Li, R. Jin, C.A. Mirkin, and R.L. Letsinger, *Nucleic Acids Res.*, 2002, 30, 1558-62.
11. L.M. Demers, et al., *Anal Chem*, 2000, 72, 5535-5541.
12. R.L. Letsinger, R. Elghanian, G. Viswanadham, and C.A. Mirkin, *Bioconjugate Chemistry*, 2000, 11, 289-291.

Ordering Information

Conjugation & Surface Attachment Modifications

Product	Catalog No.	50 nmol scale (XX=05)	200 nmol scale (XX=02)	1 μ mol scale (XX=01)	2 μ mol scale (XX=03)	10 μ mol scale (XX=10)	15 μ mol scale (XX=15)
Alkyne-Modifier Serinol	26-6925	\$240.50	\$240.50	\$312.65	\$468.97	\$2,501.20	\$3,126.50
Alkyne-NHS	26-6924	\$90.00	\$90.00	\$117.00	\$175.50	\$936.00	\$1,170.00
Amino C6 U (RNA)	27-6422	\$720.00	\$720.00	\$936.00	\$1,404.00	\$7,488.00	\$9,360.00
Amino deoxyadenosine dA C6	26-6666	\$225.50	\$225.50	\$293.15	\$438.75	\$2,345.20	\$2,931.50
Amino doxycytosine dC C6	26-6670	\$247.50	\$247.50	\$321.75	\$482.62	\$2,574.00	\$3,217.50
Amino deoxythymidine dT C6	26-6438	\$216.00	\$216.00	\$280.80	\$421.20	\$2,246.40	\$2,808.00
Amino Linker C12	26-6420	\$117.00	\$117.00	\$152.10	\$228.15	\$1,216.80	\$1,521.00
Amino Linker C3	26-6405	\$65.00	\$65.00	\$84.50	\$126.75	\$676.00	\$845.00
Amino Linker C6	26-6418	\$78.00	\$78.00	\$101.40	\$152.10	\$811.20	\$1,014.00
Amino Linker C7	26-6406	\$123.50	\$123.50	\$160.55	\$240.82	\$1,284.40	\$1,605.50
Amino modifier serinol	26-6715	\$247.50	\$247.50	\$321.75	\$482.62	\$2,574.00	\$3,217.50
Azidobutyrate NHS	26-6922	\$90.00	\$90.00	\$117.00	\$175.50	\$936.00	\$1,170.00
Carboxy-C10	26-6717	\$64.00	\$64.00	\$96.00	\$144.00	\$720.00	\$936.00
Carboxy-deoxythymidine dT	26-6697	\$216.00	\$216.00	\$280.80	\$421.20	\$2,246.40	\$2,808.00
Maleimide-Modifier (5')	26-6574	\$144.00	\$144.00	\$216.00	\$354.00	\$1,728.00	\$2,592.00
PC Amino C6 (Photocleavable)	26-6690	\$170.00	\$170.00	\$210.00	\$330.00	Inquire	Inquire
Thiol SS Dipod (Dithiol phosphoramidite (DTPA))	26-6667	\$410.00	\$410.00	\$500.00	\$725.00	\$3,130.00	\$3,410.00
Thiol SS-C3	26-6482	\$210.00	\$210.00	\$290.00	\$395.00	\$2,127.00	\$2,450.00
Thiol SS-C6	26-6419	\$125.00	\$125.00	\$290.00	\$395.00	\$2,127.00	\$2,450.00

Warranty and Liability

Information in this document is subject to change without notice. This document and all information presented in this document are written as a guide. Gene Link, Inc. does not warrant this document to be free of errors and assumes no responsibility for any errors that may appear in this document.

Gene Link disclaims all warranties with respect to this document, expressed or implied, including but not limited to those of merchantability or fitness for a particular purpose. In no event shall Gene Link be liable, whether in contract, tort, warranty, or under any statute or on any other basis for special, incidental, indirect, punitive, multiple or consequential damages in connection with or arising from this document, including but not limited to the use thereof.

Research Use Only. Not for use in diagnostic procedures.

Notice to Purchaser: The purchase of this product conveys to the purchaser the limited, non-transferable right to use the purchased amount of the product only to perform internal research for the sole benefit of the purchaser. No right to resell this product or any of its components is conveyed expressly, by implication, or by estoppel. This product is for internal research purposes only and is not for use in commercial applications of any kind, including, without limitation, quality control and commercial services such as reporting the results of purchaser's activities for a fee or other form of consideration. For information on obtaining additional rights, please contact sales@genelink.com.

© 2014 Gene Link Inc. All rights reserved.

The trademarks mentioned herein are the property of their respective owners.

Fabrication and Use of Electroless Plated Polymer Surface-Enhanced Raman Spectroscopy Substrates for Viral Gene Detection

Niranjan A. Malvadkar,[†] Gokhan Demirel,[†] Mary Poss,[‡] Ali Javed,[§] Walter J. Dressick,^{||} and Melik C. Demirel^{*;†}

Department of Engineering Science and Infectious Disease Center, Pennsylvania State University, University Park, Pennsylvania 16802, [Gene Link, Hawthorne, New York 10532](#), and Naval Research Laboratory, Code 6910, 4555 Overlook Avenue, S.W., Washington, DC 20375

Received: February 20, 2010; Revised Manuscript Received: May 6, 2010

Surface-enhanced Raman spectroscopy (SERS) substrates are prepared by electroless Ag metallization and vapor phase Au deposition on nanostructured poly(chloro-*p*-xylylene) (nanoPPX) templates. These substrates exhibit quasi-periodic nanomorphology inherited from the underlying nanoPPX template, resulting in highly reproducible SERS signal (<10% spot-to-spot and substrate-to-substrate signal variation for Au/nanoPPX comprising contributions from substrate imperfections). These substrates are therefore chosen for developing respiratory syncytial virus (RSV) gene detection that requires high sensitivity, stability, and reproducibility of the Raman signal. Metallized nanoPPX films show enhancement factors of $\sim 10^4$ to 10^6 that strongly depend on the metallization route and can be optimized by controlling the metallization parameters. RSV gene detection is achieved by using a molecular probe (MP) consisting of a fluorescent moiety and a thiol linker for attachment to the SERS substrate. To detect multiple targets, MPs are designed in two colors (Hex and Cy5 dyes) utilizing a broad range of fluorophores. Our approach provides reproducible dual-mode detection (i.e., fluorescent and SERS) where the assay results generated by fluorescence and SERS are self-confirmatory and eliminate false positives.

1. Introduction

Ever since its discovery and verification in the 1970s,^{1–3} surface-enhanced Raman spectroscopy (SERS) has become very popular among surface scientists due to its ability to characterize molecular monolayers, interfacial reactions, and biological surfaces. Despite such popularity, there are several problems in using SERS as a diagnostic tool, such as false-negative/false-positive identification of the analyte, especially for large biomolecules and microorganisms, low signal enhancement, and irreproducibility. It was soon realized that there is a strong correlation between the signal enhancement properties, such as the enhancement factor (EF) and signal repeatability and stability, with the morphology of the SERS-active metals such as Au and Ag. Although enhancement can be achieved on rough SERS-active metals prepared by any conceivable method, challenges lie in fabricating these surfaces with high consistency, reproducibility, and stability to achieve reliable repeatability in the SERS signal. The rapid development in nanoscience and nanotechnology in the past two decades has renewed interest in SERS due to its potential to overcome these barriers.

Facile synthesis of Au and Ag nanoparticles is possible via wet chemical routes through controlled reduction of their respective ions, producing size-controlled SERS templates that exhibit large enhancement. The extensive literature on using Au and Ag nanoparticles in SERS suggests that besides the size, factors such as particle size variation, shape,^{4–6} and the state of

aggregation⁷ have a great impact on the enhancement properties. Given the importance of particle spacing in the SERS, a good control over organization of nanoparticles is necessary. Stabilizing the colloidal nanoparticles on a surface was proposed as a possible method to control the enhancement properties.⁸ Various methods such as nanosphere lithography,⁹ layer-by-layer assembly,^{10,11} self-assembly,¹² or deposition of Au or Ag nanoparticles on ceramic nanorods,¹³ polymeric nanorods,¹⁴ anodic aluminum oxide nanochannels,¹⁵ and optical fibers¹⁶ have been employed to build three-dimensional architectures of Au or Ag nanoparticle structures.

We recently reported the fabrication of aligned, tilted poly(chloro-*p*-xylylene) nanorod arrays (nanoPPX) via a bottom-up approach called oblique angle polymerization (OAP),^{17–19} which does not require any lithography or masking. A nanoPPX film coated with a thin metal (e.g., Ag or Au) film via vapor phase deposition techniques provides reproducible SERS signals using standard instrumentation (note Experimental Section; <10% intensity variation from spot-to-spot and substrate-to-substrate measurements comprising approximately equal contributions from instrument sources and substrate heterogeneity).¹⁴ These important characteristics of the SERS substrate make it an ideal candidate for use as SERS-based biosensors. For instance, we showed that pathogenic bacteria and viruses can be detected with excellent sample-to-sample reproducibility and low detection time (~ 10 s spectral acquisition time).¹⁴ Despite these encouraging results, the potential of this detection technology is limited by the nonspecific binding of analytes to naked metallic nanoparticles. We therefore explore the molecular probe (MP)-based detection approach, which is highly specific to a target DNA, in this paper. In addition to vapor phase metal deposition on nanoPPX films, we also test wet chemical approaches, specifically, electroless metal deposition techniques,

* To whom correspondence should be addressed. Tel: 814-863-2270. Fax: 814-865-9974. E-mail: mdemirel@enr.psu.edu.

[†] Department of Engineering Science, Pennsylvania State University.

[‡] Infectious Disease Center, Pennsylvania State University.

[§] Gene Link.

^{||} Naval Research Laboratory.

to prepare SERS substrates. Because electroless deposition (ED) can produce conformal metal films on catalyzed planar²⁰ or nonplanar^{21,22} surfaces under ambient conditions via direct metal growth, differences in metal film morphology and coverage that can affect SERS response as compared to vapor-metallized substrates are expected. In addition, in contrast to vapor-based metallization, electroless processes are inexpensive and readily automated, simplifying large-scale substrate manufacture.

We describe here three methods to prepare SERS substrates on nanoPPX films: (1) ED by treating the nanoPPX films with a commercial Pd/Sn catalyst and then metallizing the surface using an electroless Ag bath; (2) ED by first treating the nanoPPX films with an adhesive component (ligand) that binds a Sn-free Pd^{II}-based catalyst and then metallizing the surface using the Ag bath; and (3) vapor phase deposition of Au. Structural characterization is performed using field-emission scanning electron microscopy (FESEM), transmission electron microscopy (TEM), and atomic force microscopy (AFM), while the EF of SERS substrates is measured using 4-fluorobenzenethiol (FBT). Furthermore, we describe a metal growth model correlating the EF to the morphological characteristics of the substrates. From the substrates prepared by the routes mentioned above, we select two substrates, based on their morphology and enhancement properties, for detecting the respiratory syncytial virus (RSV) gene sequence by means of a MP bearing a fluorescent moiety.

2. Experimental Section

2.1. Materials. Deionized water of 18.1 MΩ cm was used for all experiments using a Barnstead Nanopure Diamond dispenser. Dichloro-[2,2]-paracyclophane, the precursor for nanoPPX deposition, was purchased from Parylene Distribution Services (PDS) Inc., TX. The *p* type Si(100) wafers were purchased from Wafernet Inc. (San Jose, CA) and were used as substrates for nanoPPX deposition. Pd/Sn catalyst components, CATAPREP 404 (stabilizer), CATAPOSIT 44 (Pd/Sn concentrate), and Accelerator 19 (reaction accelerator), were purchased from Rohm and Haas (Shibley Co.) and were used as instructed by the manufacturer. Electroless Ag bath components, AgNO₃, (NH₄)₂SO₄, CoSO₄·7H₂O, and aqueous ammonia, and Sn-free Pd catalyst components, Na₂PdCl₄·3H₂O, 2-(*N*-morpholino)ethanesulfonic acid (MES) buffer, and NaCl, were ACS reagent grade and were used as received.

2.2. NanoPPX. Si(100) (Wafernet Inc.) wafers were used as the substrate to deposit the nanoPPX films. Wafers were cleaned, and a self-assembled monolayer (SAM) of allyltrimethoxysilane was deposited per the procedure used in our previous work.²³ SAM-functionalized wafers were stored in a dark container at a temperature of 4 °C until required for the polymer deposition. For nanoPPX deposition, we modified the method employed by Gorham²⁴ involving deposition of PPX films using a low pressure, vapor deposition technique.¹⁸ Dichloro-[2,2]-paracyclophane (PDS Inc., TX) was used as the precursor for the deposition. A 0.3 g portion of the precursor was sublimed at a temperature of 175 °C under a pressure of ~10 milli-Torr. The precursor vapor was then pyrolyzed at 690 °C. The pyrolysis of dichloro-[2,2]-paracyclophane results in the cleavage of the alkyl bridge to form chloro-*p*-quinodimethane (or chloro-*p*-xylylene) ↔ diradical. The diradical flux when directed at an angle of 10° on the silicon substrate results in a low-density porous PPX film with a unique aligned nanorod morphology.¹⁷

2.3. Electroless Reagents. NanoPPX films were subjected to Ag metallization using two different routes: (A) using Pd/Sn

catalyst followed by plating in Ag bath and (B) using Sn-free Pd catalyst followed by plating in Ag bath. The preparation of various electroless reagents used for Ag metallization is described below.

2.3.1. Pd/Sn Catalyst. Pd/Sn catalyst was freshly prepared just before use. To prepare the Pd/Sn catalyst, 10 g of CATAPREP 404 stabilizer (Shibley Inc.) was weighed and dissolved in ~45 mL of H₂O. This solution was transferred to a 50 mL volumetric flask. A 1.5 mL amount of CATAPOSIT 44 Pd/Sn concentrate (Rohm and Haas, Shibley Inc.) was then added using a micropipet and diluted to the mark using H₂O. The flask was tightly sealed because the colloid is O₂ sensitive if exposed to air for extended times.

2.3.2. Sn-Free Pd Catalyst. Sn-free Pd catalyst was prepared per the procedure described for PD1 in Dressick et al.²⁵ Briefly, 11.5 mg of Na₂PdCl₄·3H₂O was completely dissolved in 1 mL of 1 M aqueous solution of NaCl in a 100 mL volumetric flask. Later, 10 mL of pH 5 0.1 M MES buffer solution was added to the flask. H₂O was added to dilute the solution up to the mark. The solution was incubated at 25 ± 0.1 °C in a temperature-controlled water bath for 24 h, after which a 10 mL aliquot of the dispersion was removed and replaced with 10 mL of the 1 M NaCl solution. The resultant PD1 catalyst dispersion remains stable for up to at least 1 month in the water bath held at 25 ± 0.1 °C.

2.3.3. Electroless Ag Bath. An electroless Ag bath was also freshly prepared before each experiment. To prepare the bath, 0.7 g of AgNO₃ and 10 g of (NH₄)₂SO₄ were dissolved in 70 mL of H₂O, and the resulting solution was added to a 100 mL volumetric flask. Aqueous ammonia (28%, w/w) was added to dilute the solution up to the mark. A 2.8 g amount of CoSO₄·7H₂O was then added to the solution. The resultant composition of the bath was AgNO₃ (0.05 M), (NH₄)₂SO₄ (0.9 M), NH₃ (2.1 M), and CoSO₄·7H₂O (0.12 M), pH 10.

2.4. Preparation of SERS Substrates. 2.4.1. Scheme A: Direct Ag Metallization Using Pd/Sn. NanoPPX films were treated with Pd/Sn catalyst for 10 min. Excess catalyst was carefully removed using a Pasteur pipet. The films were then gently rinsed in 0.12 M HCl (aq) solution for 5–10 s. Care was taken not to pour the HCl solution directly on the film, as it can remove the bound Pd/Sn catalyst. Immediately after HCl treatment, the films were immersed in the 10% Accelerator 19(aq) solution for 30 s. Films were removed from the Accelerator solution, washed in H₂O, and transferred to the electroless Ag bath. The plating bath was gently agitated to ensure uniform deposition of Ag onto the nanoPPX films. Plating was carried out for various times ranging from 5 to 120 min.

2.4.2. Scheme B: Direct Ag Metallization Using PD1. NanoPPX films were first soaked in 1 M pyridine(aq) solution for ~48 h. The films were then washed in H₂O, dried under N₂ gas, and transferred to the PD1 dispersion. After the treatment of the films in PD1 dispersion for 45 min, an excess PD1 dispersion was carefully removed using a Pasteur pipet. Films were then gently washed in H₂O for 5–10 s and transferred to the electroless Ag bath. The plating bath was gently agitated to ensure uniform deposition of Ag onto the nanoPPX films. Plating was carried out for various times ranging from 5 to 150 min.

2.4.3. Scheme C: Vapor Phase Deposition of Au. In addition to preparing Ag substrates via the above schemes, we also prepared SERS substrates by coating nanoPPX films with thermally evaporated Au or Ag. The metal (in wire form) placed in Ta boats was resistively heated in a chamber maintained at

TABLE 1: Designed RSV Probes

synthetic positive control template (SPCT)	TTTGGTGGTGTGATGGTTGGCTCTTCTGTGGGCTTGGTG	G probe complementary in M11486: 5321–5360
G gene from RSV	CGCAGCCACAGAAGAGCCAACCATCAACACTGCG	G probe position in M11486: 5329–5352

TABLE 2: Modifications and Synthesis

probe name	GL designed probes final	3' mod (details)
SPCT	TTTGGTGGTGTGATGGTTGGCTCTTCTGTGGGCTTGGTG	
SC6-Hex	CGCAGCCACAGAAGAGCCAACCATCAACACTGCG7	SS-C6 (3'-SH-C6-oligo-Hex)
SC6-Cy5	CGCAGCCACAGAAGAGCCAACCATCAACACTGCG7	SS-C6 (3'-SH-C6-oligo-Cy5)
S2-Hex	CGCAGCCACAGAAGAGCCAACCATCAACACTGCG8	dithiol (dipod) (3'-SH-C4-SH-C3-oligo-Hex)
S2-Cy5	6CGCAGCCACAGAAGAGCCAACCATCAACACTGCG8	dithiol (dipod) (3'-SH-C4-SH-C3-oligo-Cy5)

TABLE 3: Viral Gene Sequence from RSV

entry	sequence (5'–3')
RSV G-gene (sense strand 5'–3')	AAAGGAAGTACCCACCACCAAGCCACAGAAGAGCCAACCATCAACACCACCAAAACAAAC ATCATAACTACACTACTCACCTCCAACACCACAGGAAATCCAGAACTCACAAGTCAAATGGA AACCTTCCACTCAACTTCTCT

$\sim 1 \times 10^{-8}$ Torr base pressure. The growth of the metal layer, monitored by a parallel quartz crystal microbalance (QCM), was allowed to continue until a thickness of 60 nm was reached.

2.5. Characterization. FESEM images of the film surface were taken using a JEOL 6700F FESEM operated at 3 kV accelerating voltage. TEM samples were prepared by scraping the Ag particles off of the PPX surface, suspending in ethanol, and sonicating the suspension for ~ 20 min. A drop of this suspension was added to a carbon-coated copper grid and allowed to dry in air. TEM images were obtained using Philips (FEI) EM420T TEM operated at an accelerating voltage of 120 kV. TEM images were analyzed for Ag particle size distribution using ImageJ software program. Nanostructured surface morphology was characterized by an atomic force microscope (Nanoscope E, Veeco) using contact mode silicon nitride cantilevers (Veeco Metrology, CA).

2.6. RSV Hairpin Probe Design. A probe sequence from the RSV genomic sequence (Accession Number: M11486) was selected corresponding to the G protein sequence from 5329 to 5352 bp (Table 1). This sequence was evaluated for minimal secondary structures and loop and dimer formation using Gene Runner DNA analysis software (www.genelink.com). The nearest neighbor T_m of the probe was 60 °C. A hairpin sequence was added to the 5'- and 3'-end of the sequence that yields a stable hairpin structure without creating loop and secondary structures with the target loop sequence. The 5'-end of the hairpin probe sequence was either labeled with hexachlorofluorescein (Hex) or cyanine 5 (Cy5) dye. The 3'-end was modified with two thiol linker groups. Structures of the dyes and thiol linkers are discussed further in section 3.4 of the text.

2.7. Probe Modification. The hairpin probe DNA sequences were synthesized at Genelink with two thiols (i.e., SC6 and S2) and two 5'-fluorophores (i.e., Hex and Cy5) containing sequence as detailed in Table 2. These probes were synthesized using 3'-thiol C6 CPG or 3'-dithiol CPG (Glen Research, VI) as the solid support followed by the oligo sequence and coupled to either Hex or Cy5 dyes. The crude probes obtained after complete deprotection were ethanol precipitated and polyacrylamide gel purified. Immobilization of DNA, unless otherwise stated, was carried out as follows: Prior to immobilization steps, the SERS substrates were cleaned in a UV/ozone chamber oxidative medium for ~ 2 min. Different concentrations (10^{-10} – 10^{-6} M) of probe DNA in a buffer solution (50 mM KCl, 10 mM Tris-HCl, and 1.5 mM MgCl₂ and pH 8.0) were prepared, and a drop of each solution was placed on the SERS substrates. Immobilization of probe DNA on the SERS substrate

was allowed to proceed for ~ 24 h at room temperature. Afterward, the surfaces were washed several times with the buffer solution and dried under air stream.

2.8. Purification of RSV Genomic RNA. RSV strain A2 was propagated in HEp-2 cells. Supernatant containing infectious virus particles was harvested, and viral genomic RNA was isolated using QIAamp viral RNA mini kit (Qiagen Corp., Valencia, CA). The viral gene sequence from RSV is listed in Table 3.

2.9. Hybridization Assay. Hybridization was carried out by adding 100 μ L of complementary synthetic DNA or genomic RNA (at least 4-fold of MP concentration) onto the surfaces. The hybridization assay was allowed to react for 10 min to 3 h in a dark and ambient environment. Afterward, the assay was rinsed with the buffer solution and dried under an air stream.

2.10. Fluorescence Measurements. An Olympus Fluoview 300 confocal laser scanning microscope with two single-line lasers (Green Ar-ion, 515 nm, and Red HeNe, 633 nm) was used with two different objectives (PlanApo 60 \times and UplanFL 40 \times) for imaging. After imaging on a confocal microscope, the total intensity was measured using FLUOVIEW software.

2.11. SERS Measurements. FBT (Caution: There is a stench from FBT. Use only in a well-ventilated fume hood.) was used as the analyte to measure the SERS enhancement and signal uniformity of the substrates. The analyte solution was prepared by dissolving 20 μ L of FBT in 20 mL of ethyl alcohol. Ag-coated nanoPPX films were immersed in the FBT solution immediately after Ag deposition and stored overnight in a sealed vial. Afterward, the films were removed and rinsed in ethyl alcohol for 1 min to remove any physisorbed FBT molecules. The films were stored in sterilized Petri dish until required for SERS characterization. We used Renishaw inVia microRaman equipped with 35 mW HeNe laser ($\lambda = 632.8$ nm) and Ar ion ($\lambda = 514.5$ nm) lasers for SERS characterization. For each sample, the 50 \times objective lens and a 10 s acquisition time were used. For normalization of SERS spectra due to the variation in the acquisition power, a Raman spectrum of Si (100) was used as the reference.

3. Results and Discussion

3.1. Fabrication of SERS Substrates. The OAP technique for vapor phase deposition of nanoPPX films has been studied in detail in our previous works.^{17,18} Briefly, direction of the diradical flux, formed via vapor phase thermolysis of a *p*-cyclophane precursor, onto a substrate surface at a low incidence angle (i.e., $\sim 10^\circ$) leads to surface polymerization and formation

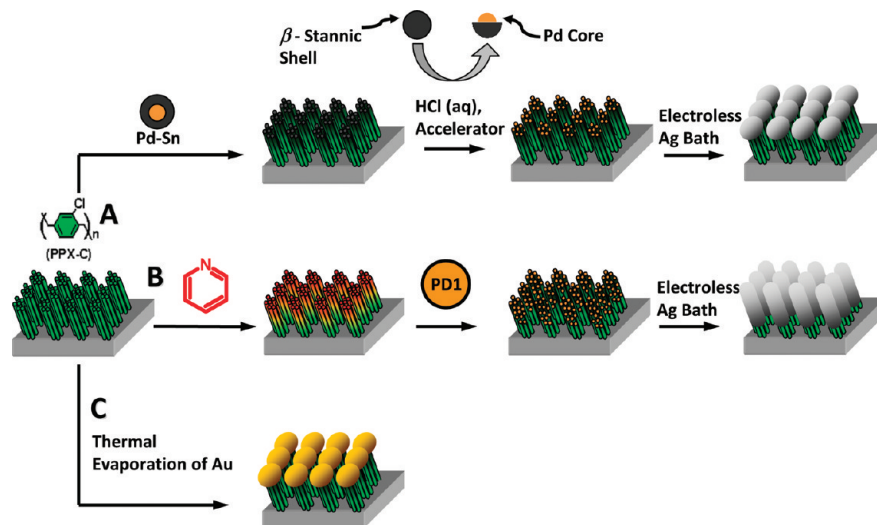


Figure 1. NanoPPX-templated SERS substrates prepared via (A) commercial Pd/Sn catalyst treatment, (B) noncovalent pyridine adsorption followed by PD1 treatment, and (C) thermal evaporation of Au.

of a parylene nanorod structure (note the Figure 1 scheme). The growth of the film by OAP occurs via preferred growth of certain nuclei on the surface and suppressed growth of the rest leading to oriented crystallization of the polymeric material on the substrate. The growth is controlled by the self-shadowing effect and surface diffusion. While the self-shadowing phenomenon is entirely a physical effect occurring due to the geometry of the substrate orientation and the monomer flux, surface diffusion, on the other hand, is dependent on the temperature and the surface chemistry of the material deposited and the substrate. Consequently, the morphological parameters of the film such as column diameter, column separation, and column height can be controlled by tuning the deposition parameters and/or the monomer chemistry.^{17,18} In this work, we kept the deposition parameters in the OAP process constant while varying the subsequent metallization routes/conditions to prepare various SERS substrates.

Figure 1 shows the three routes used to prepare SERS substrates using electroless (schemes A and B) and vapor phase (scheme C) metallization routes. Scheme A uses a commercial Pd/Sn core/shell colloidal species to catalyze the nanoPPX surface. The β -stannic shell of the colloid binds the colloid onto the polymer surface via noncovalent forces such as van der Waals interactions. Later, the catalytic Pd⁰ core is exposed by treatment with an “acceleration” agent (e.g., fluoroboric acid) that removes a portion of the β -stannic shell. After the Pd⁰ core is exposed, the films are transferred to the Ag bath where reduction of Ag takes place on the catalytic Pd⁰ sites.

Scheme B depicts a noncovalent ligand functionalization strategy to stabilize Ag nanoparticles on the PPX nanorods, previously implemented for preparing highly porous Ni,²² Co,²³ and TiO₂²⁶ films. We took advantage of the highly porous and amorphous nature²⁷ of the nanoPPX film to physisorb aromatic ligand molecules such as pyridine that are stabilized via π - π interactions with the aromatic moieties of the nanoPPX.²² Subsequently, PD1, a catalytic Pd(II)-based colloidal dispersion, is allowed to covalently bind to the pyridine-functionalized nanoPPX films.^{28,29} PD1 nanoparticles act as the catalytic sites where nucleation and growth of Ag nanoparticles occur. It should be noted that although the underlying pyridine ligands are bound to the parylene nanorods by weak π - π interactions, an array of such interactions can produce enough attraction to stabilize them on the polymer surface, which is manifested in

the Scotch tape adhesion test resulting in less than 5% metal removal after PD1 binding and electroless metal deposition. SERS substrates prepared by this route therefore show enhanced stability and robustness as compared to substrates prepared via scheme A, in which the metal particles are bound via much weaker van der Waals interaction.

SERS properties of substrates prepared by vapor phase deposition of Au over the nanoPPX templates (scheme C) have been studied previously.¹⁴ Briefly, during vapor phase metallization, Au nanoparticles are immobilized on the nanorod polymer surfaces comprising the nanoPPX film. Although a highly uniform layer of Au can be deposited by vapor phase deposition that replicates the quasi-periodic morphology of the underlying nanoPPX, these composite nanostructures do not pass the Scotch tape adhesion test due to lack of strong interacting forces between the polymer and the Au particles. Nevertheless, these composite nanostructures exhibit EFs of up to $\sim 10^4$ with high substrate-to-substrate and spot-to-spot reproducibility on a large area (<10% signal variation in a 1 mm² area).¹⁴

3.2. Characterization of SERS Substrates. In the remainder of our discussion, references to films prepared by schemes A–C are taken to mean films prepared as shown in Figure 1. Figure 2A shows the FESEM image (top view) of a Ag/nanoPPX substrate prepared via scheme A. Uniform deposition of Ag particles on the nanoPPX substrate is observed, resulting in a continuous porous film. However, the particle deposition occurs only on the top of the PPX nanorods, relinquishing the underlying aligned nanorod morphology as shown in Figure 2B (side view). In contrast, Ag formation according to scheme B in Figure 2C appears to be conformal to the aligned PPX nanorods, similar to the observed morphology of Ni²² and Co²⁷ films previously grown on nanoPPX substrates via the noncovalent ligand functionalization route. Figure 2D shows a side view of the Ag-plated nanoPPX films prepared according to scheme B. The deeper penetration of the metal in the nanoPPX porous structure observed contrasts with the morphology of the Ag/nanoPPX film prepared via scheme A (Figure 2B) and contributes to the interface adhesion via mechanical metal anchoring, complementing the contribution of π - π interactions, consistent with the aforementioned Scotch tape test result. Finally, Figure 2E shows the FESEM of a Au/nanoPPX film prepared according to scheme C. In this case, vapor phase deposition of Au onto a nanoPPX substrate provides a Au layer

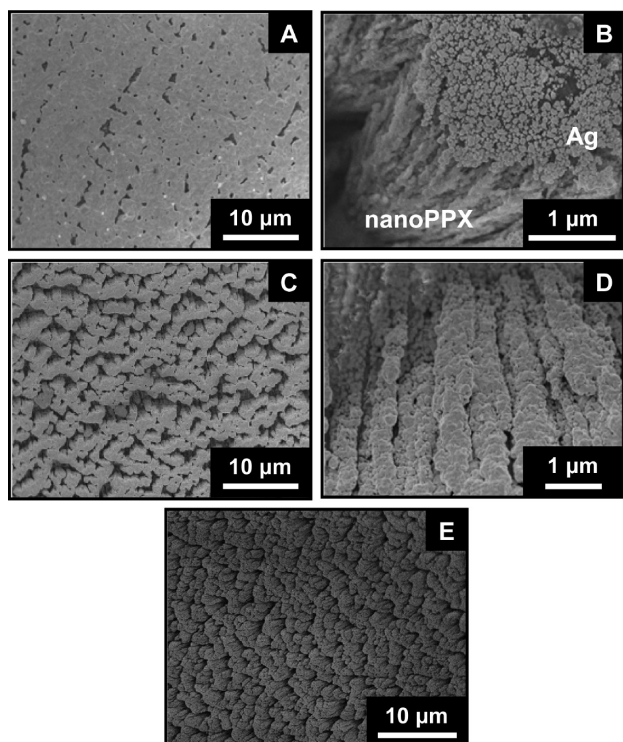


Figure 2. FESEM images (top views) of SERS-active substrates prepared via (A) scheme A (cf. sample 3 in Table 4), (C) scheme B (cf. sample 7 in Table 4), and (E) scheme C (cf. sample 9 in Table 4). Part B shows a high-magnification SEM image (side view) of the scheme A substrate prepared by 15 min of plating in a Ag bath. Particle agglomeration on top of the PPX nanorods is visible atop the unplated nanoPPX in the film interior. Part D shows a high-magnification cross-section FESEM image (side view) of the scheme B substrate plated for 60 min in a Ag bath. Conformal growth of Ag over the aligned nanorod morphology within the interior of the nanoPPX film is evident.

of thickness of 60 nm. This thin layer of Au uniformly coats the nanoPPX surface, mimicking its quasi-periodic aligned nanorod structure.

Contact mode AFM images were taken for substrates prepared via scheme B with varying plating time. The AFM images show a monotonic increase in the Ag particle size with the plating time (Figure S-1 in the Supporting Information), although exact quantification of particle size is difficult due to the tip convolution. The increase in the particle size is accompanied by a decrease in particle–particle separation from adjacent PPX nanorods.

TEM analyses provide a quantitative measure of the Ag particle size distribution for the three types of substrates. All TEM images (Figure 3) show Ag or Au metal nanoparticles bound by the PPX matrix. Particle size distributions (shown in Table 4) obtained from these images show the average particle size of scheme A and B substrates to be ~ 22 and ~ 69 nm, respectively. In addition, the polydispersity, calculated as the standard deviation (σ) of particle size, of scheme B ($\sigma_B \approx 47$) is higher as compared to that of scheme A ($\sigma_A \approx 24$). The large size and polydispersity of Ag particles of scheme B substrates are inherited from the broad size distribution of PD1 particles (4–53 nm) used to catalyze the pyridine-functionalized nanoPPX film.²⁵ Moreover, the high surface coverage of pyridine on the nanoPPX surface via aqueous solution treatment also assists in binding PD1 particles with broad size range.³⁰ Pd/Sn catalyst particles, on the other hand, exhibit much lower polydispersity values as compared to PD1. Although typical Pd/

Sn catalyst particle diameters range from ~ 1 to 5 nm, aggregates occur and exhibit somewhat larger apparent polydispersity values (4–20 nm).²¹ Consequently, Ag plating on nanoPPX films catalyzed by the Pd/Sn catalyst exhibits smaller average Ag particle sizes and particle distributions than Ag films plated using the PD1 catalyst.

We used FBT to determine the SERS EFs for the various metallized nanoPPX samples of Table 4. Figure 4A,B shows the SERS spectrum of FBT adsorbed on Ag/nanoPPX substrate prepared via schemes A and B, respectively. A bulk Raman spectrum of FBT is shown in Figure 4C for comparison. The major difference between the SERS and the bulk Raman spectrum is the absence of the 918 cm^{-1} peak corresponding to the $\delta(\text{C-S-H})_{\text{bend}}$ mode. The absence of the 918 cm^{-1} peak is due to the deprotonation of FBT resulting in the formation 4-fluorobenzenethiolate that is adsorbed onto the Ag surface. Similar observations were reported in previous SERS studies of FBT.^{31,32} The $\nu(\text{C-F})_{\text{stretch}}$ peak at 1074 cm^{-1} observed in the SERS spectrum of FBT was used to calculate the EF for the substrate. The EF is given by:

$$\text{EF}(50 \times 1074\text{ cm}^{-1}) = \frac{N_{\text{bulk}} I_{\text{poly}}}{N_{\text{poly}} I_{\text{bulk}}} \quad (1)$$

where I_{bulk} and I_{poly} are measured intensities of FBT determined by confocal microscopy ($50\times$ objective) in bulk Raman and SERS mode, respectively, while N_{bulk} and N_{poly} are the number of molecules in the bulk and adsorbed on metallized nanoPPX substrate, respectively. The Si phonon peak at 521 cm^{-1} was used as a basis of normalization of the SERS spectrum. N_{bulk} is estimated to be $\sim 4.6 \times 10^9$, based on the density of FBT (1.197 g/cm^3) and the volume of the focal region produced by the confocal optics. N_{poly} is calculated to be $\sim 10^5$ based on a $1\text{ }\mu\text{m}$ diameter circular area of the sample surface exposed to the incident beam. $I_{\text{poly}}/I_{\text{bulk}}$ is approximated to 1/15.

EFs obtained on substrates prepared via schemes A–C are listed in Table 4. It is striking that substrates prepared using scheme A and B show a similar trend for EF variation with respect to Ag plating time, although scheme A substrates show EF values are approximately an order of magnitude lower as compared to those exhibited by scheme B substrates (Figure 4D). The highest EF achieved for both types of substrates occurs on samples that are plated for 60 min in Ag bath. The similarities and differences of the EF variation can be explained by studying the size distribution of their respective catalytic seed layer used in preparing the substrates and their Ag coverage on the nanoPPX templates (vide infra). The EF of scheme C substrates, on the other hand, depends on the thickness of the Au layer deposited and reaches a maximum of $\sim 1 \times 10^5$ for 60 nm thickness of Au and decreases as further metal is deposited.¹⁴ It is interesting to note that such a trend is similar to the one observed for substrates prepared via schemes A and B.

3.3. Metal Growth Model. We describe herein a model correlating the observed variation of the EF and the growth of the Ag particles, specifically those prepared via electroless metallization (i.e., schemes A and B). Our model is partially substantiated by structural characterization (i.e., FESEM, AFM, and TEM studies) and previously studied geometry of the PPX nanorod growth.¹⁷ For Ag/nanoPPX films prepared via schemes A and B, the low EFs for substrates plated for less than 30 min reflects the low coverage of Ag on the nanoPPX templates. At these plating times, the Ag nanoparticles are small and have high curvatures, as observed by AFM (Figure S-1 in the

TABLE 4: Comparison of the SERS Substrates

sample no.	metal deposition scheme	catalyst used	catalyst time (min)	metallization time (min) (metal)	Ag (or Au) particle size ($D_{\text{average}} \pm \sigma$)	mean EF
1	A	Pd/Sn	10	5 (Ag)		6.8×10^2
2	A	Pd/Sn	10	30 (Ag)		1.4×10^4
3	A	Pd/Sn	10	60 (Ag)	22 ± 24	6.1×10^4
4	A	Pd/Sn	10	150 (Ag)		3.8×10^4
5	B	PD1	45	5 (Ag)		2.1×10^4
6	B	PD1	45	30 (Ag)		2.5×10^5
7	B	PD1	45	60 (Ag)	69 ± 47	3.0×10^5
8	B	PD1	45	150 (Ag)		1.2×10^5
9	C	none	N/A	~ 2 (Au) ^a	34 ± 16	1.0×10^5
10	C ¹⁴	none	N/A	~ 2 (Ag) ^a	38 ± 10	1.0×10^6

^a An ~ 2 min deposition time \equiv 60 nm thickness (QCM monitored).

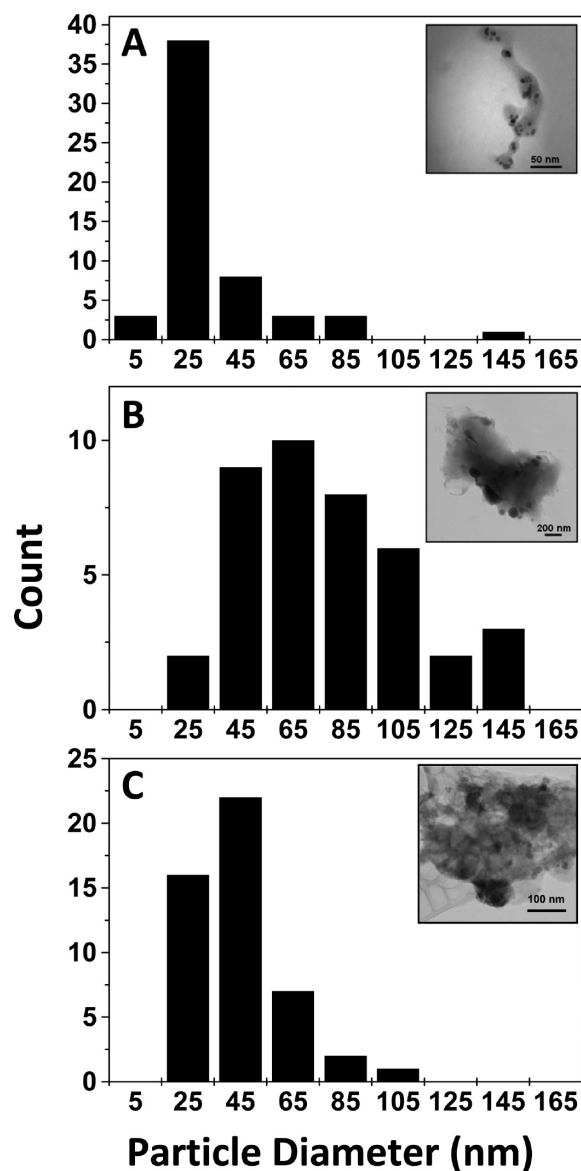


Figure 3. Particle size distribution obtained from TEM images (shown as insets) of scraped-off metal particles deposited on nanoPPX film via (A) scheme A (cf. sample 3 in Table 4), (B) scheme B (cf. sample 7 in Table 4), and (C) scheme C (cf. sample 9 in Table 4).

Supporting Information), which are derived from the size of the Pd catalysts used. Moreover, at lower plating times, the Ag particle–particle separation between adjacent nanorods is too large for efficient interaction of their plasmon electromagnetic fields required for “hot spot” formation on the surface. The

enhancement achieved is only due to the curvature of the Ag particles and/or the formation of a few “hot spots” due to particle agglomeration within a single PPX nanorod. At ~ 60 min of plating time, the distance between growing metal fronts on adjacent PPX nanorods are very close to each other. The gaps between these two metal fronts are now close enough for “hot spot” formation. FBT molecules bound in these gaps experience strong electromagnetic fields during SERS excitation and therefore show the highest EFs. At plating times greater than 60 min, the Ag particle growth fronts increasingly physically encounter growth fronts from Ag particles on adjacent PPX nanorods. As a result, the growing metal fronts merge with one another forming a continuous porous Ag film. Because of this fusion of Ag particles, the FBT molecules are restricted primarily on the surface of the film. Therefore, the only contribution to the enhancement at this stage is due to the nanoscale roughness of the Ag film alone, leading to the observed saturation of EF.

The difference in the EFs between Ag/nanoPPX films prepared according to schemes A and B, on the other hand, arises due to the difference in their morphologies and particle size distributions. The growth of Ag particles in scheme B substrates occurs uniformly along the length of the PPX nanorods (Figure 2D), which typically exhibit average rod diameters and spacings of ~ 140 – 150 and ~ 40 – 50 nm, respectively. However, Ag films thicker than the average nanorod separation distance, as required for optimal SERS EF (i.e., 69 nm thick Ag, Table 4 and Figure 4D), are readily deposited. This behavior is a consequence of nanorod flexibility arising from their high aspect ratios (i.e., height/diameter > 100) and largely amorphous nature (e.g., Young’s modulus, $E = 50$ MPa).³³ Therefore, nanorod bundling can readily occur, driven by stresses introduced as aqueous solutions penetrate the hydrophilic, pyridine-impregnated nanorod films during the metallization treatments, to increase the effective spacing available for Ag deposition. Micrometer-scale distortions within confined (helical) pyridine-impregnated PPX nanostructures have been observed previously following electroless Ni metallization, consistent with our observations and arguments here (cf. Figures 1C and 3D, ref 22).²²

The growth of Ag particles in scheme A substrates, on the other hand, occurs only on the top of the PPX nanorods. Penetration of the aqueous Pd/Sn catalyst dispersion into the hydrophobic nanoPPX film (water contact angle $\sim 120^\circ$)³⁴ is inhibited in the absence of bound pyridine ligand. As a result, much of the contribution to the EF is due to particle agglomeration on top of the PPX nanorods (note Figure 2A,B). Moreover, Raman enhancement studies on single Ag nanoparticles by Emory et al. have shown that efficient enhancement using an

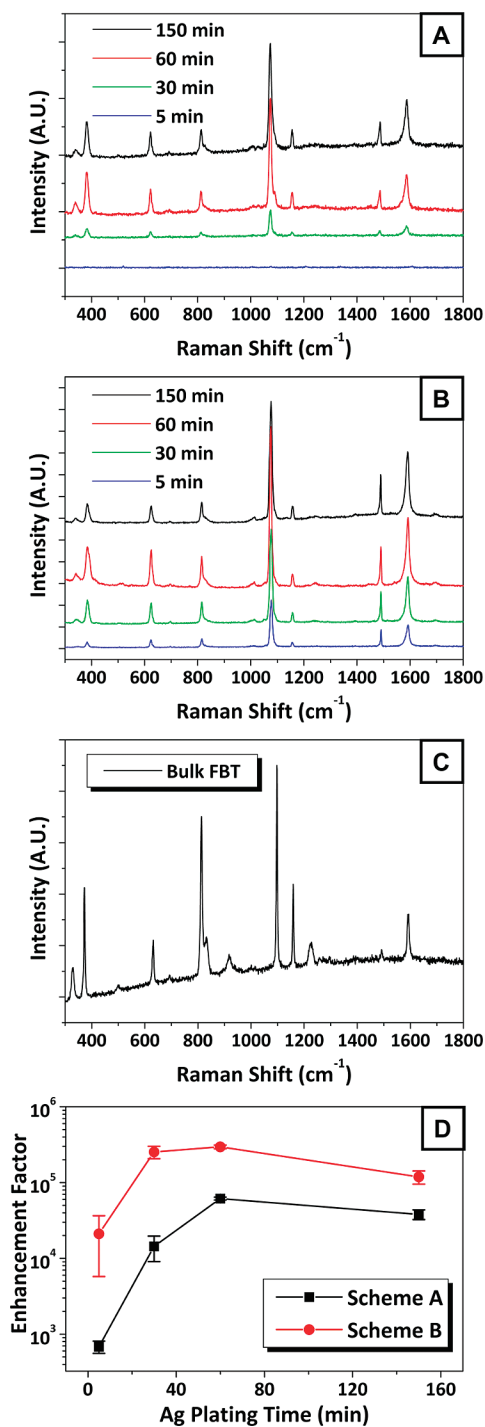


Figure 4. SERS spectra of FBT on substrates prepared via (A) scheme A and (B) scheme B. (C) Raman spectrum of pure FBT. (D) Plot of EF [calculated from $\nu(\text{C}-\text{F})$ peak at 1074 cm^{-1}] against Ag plating time.

incident laser with 647 nm wavelength, close to the one used in our study, requires particles size in the range of 190–200 nm.³⁵ Scheme B substrates show an average particle size that is closer to this range than that of scheme A substrates, consistent with the higher EF achieved in scheme B substrates. Furthermore, particle agglomeration at ~ 60 min plating time causes red shifting of the surface plasmon absorption band,³⁶ thereby inducing additional electromagnetic enhancement of the Raman signal.

3.4. RSV Gene Detection. To test the efficacy of our metal-nanoPPX films as SERS substrates, we prepared a MP-based

assay for RSV detection using metal films prepared according to schemes B and C. RSV is a virus that can cause serious infections in children and persons having weak or compromised immune systems; rapid testing and identification are of paramount importance in providing successful, prompt treatment. MPs are oligonucleotide probes that can report the presence of specific nucleic acids in homogeneous solutions or on solid substrates.³⁷ There are several advantages of using MPs for DNA/RNA detection, including no target labeling, no need to wash after hybridization, and a single hybridization step (as compared to sandwich DNA/RNA assays).³⁸ MPs typically consist of the MP oligonucleotide sequence having a hairpin structure sensitive to a complementary target oligonucleotide present in the species to be detected and a fluorescent dye and quencher attached to the 3'- and 5'-ends, respectively, of that MP oligonucleotide (Figure 5A). Our MP oligonucleotide sequence is complementary to RSV and will specifically hybridize with RNA from our viral target, RSV. Target RSVs are either a genomic RNA, which is isolated from Hep-2 cells (Table 3), or a synthetic template, which is dispersed in water before being used (Table 1). We selected two fluorophores, Hex and Cy5 dyes (Figure 5B), that have excitation peaks close to the wavelengths of two lasers built in our Raman systems (i.e., 514 and 632 nm, respectively). Two thiol linker modifiers (i.e., thiol linker, SC6, and dithiol, S2 in Figure 5B) were used to conjugate the 5'-end of our MP to the metallic SERS substrate, which acts as the dye fluorescence quencher. These dye/thiol combinations can provide four discrete MPs, as shown in Figure 5B.

In the initial nonhybridized configuration, the fluorophore is quenched by the proximity to the metal nanoparticles. When the MP encounters a complementary RSV gene target, it forms a rigid double helix, which is more stable than the stem. Subsequently, the MP undergoes a spontaneous conformational reorganization that forces the stem apart and causes the fluorophore to move away from the nanoparticle surface (i.e., hybridized configuration), leading to the restoration of fluorescence. Confocal microscopy images of nonhybridized and hybridized MPs on Au-metalized nanoPPX film (i.e., via scheme C) are shown in Figure 5C. Clearly, the hybridized configurations (i.e., open configuration of the MP when the complementary RSV gene target attached) are brighter for all cases than the nonhybridized configuration (Figure 5C insets).

Analogous detection of the hybridized and nonhybridized configurations of the MPs was performed by Raman studies of the fluorophores. Metalized nanoPPX substrates, specifically those prepared via scheme B and C, were selected for RSV gene detection, due to their highly reproducible FBT SERS spectra, using the MP with a Cy5 fluorescent moiety. Enhancement of the Raman signal of the Cy5 occurs via surface-enhanced resonance Raman scattering because the excitation wavelength is close to the electronic transition of the fluorophore. Figure 6A,C shows the SERS spectrum of the Cy5-MP (with S2 linker) on Au/nanoPPX substrate (scheme C) and Ag/nanoPPX (scheme B), respectively. When the probe hybridizes with a RSV target, the conformational reorganization separates the fluorophore from nanoparticles diminishing the SERS signal (Figure 6B,D for schemes B and C, respectively). Detection of genomic RSV RNA (instead of synthetic RSV) gives similar results (Figure S-2 in the Supporting Information). We observe four major Cy5 bands at 1594, 1500, 1271, and 1200 cm^{-1} in Figure 6C using the Au/nanoPPX SERS substrate, which corresponds to $\nu(\text{C}=\text{N})_{\text{stretch}}$, $\nu(\text{C}-\text{C})_{\text{ring}}$, and/or $\nu(\text{C}=\text{C})_{\text{ring}}$, $\nu(\text{C}-\text{N})_{\text{stretch}}$ modes, respectively. All SERS spectra for Cy5

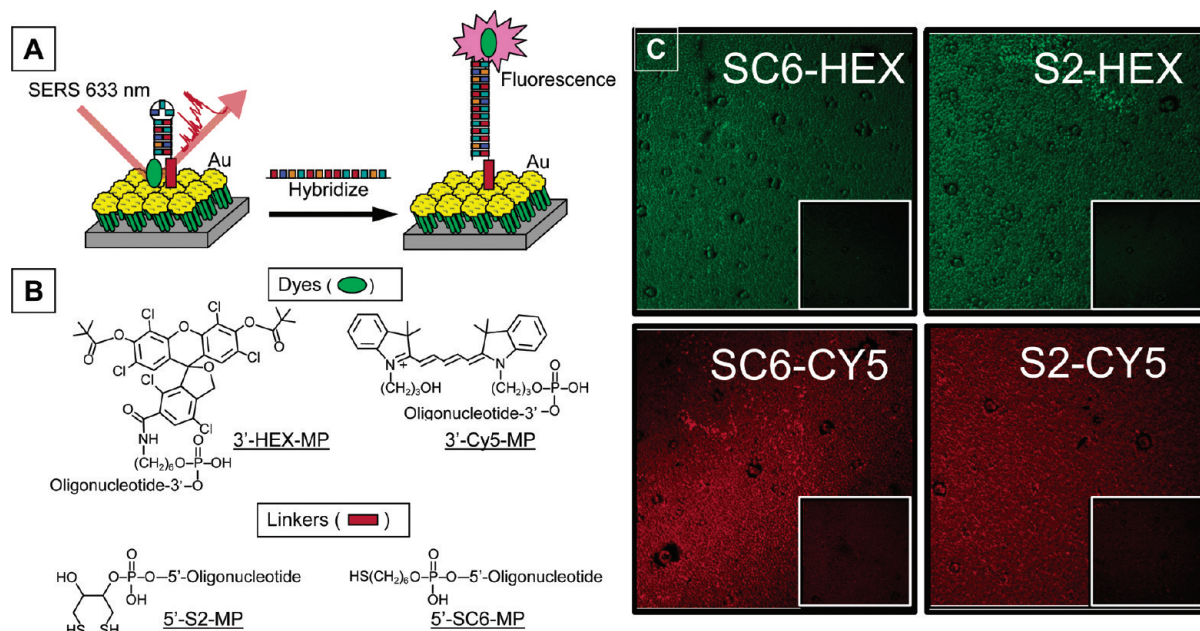


Figure 5. (A) Schematic of RSV gene detection using MP. (B) Molecular structures of the two thiol linkers, S2 and SC6, and the two fluorophores, Cy5 and Hex, used to modify the MPs. (C) Fluorescent intensities, obtained from confocal microscopy images, of the four MPs immobilized on Au/nanoPPX substrates under hybridized and nonhybridized (insets) configurations.

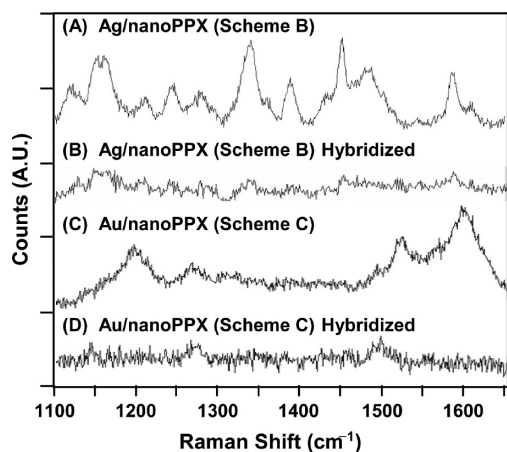


Figure 6. SERS spectrum of nonhybridized (A) and hybridized (B) Cy5-MP on Ag/nanoPPX (prepared via scheme B) and nonhybridized (C) and hybridized (D) Cy5-MP on Au/nanoPPX (prepared via scheme C). All MPs possess a SC6 linker, and all hybridized spectra are collected using synthetic RSV DNA.

match well with the literature.³⁹ We should also note that the SERS spectrum from the Ag/nanoPPX (Figure 6A) shows additional peaks (e.g., 1150, 1325, and 1390 cm⁻¹) as compared to Au/nanoPPX, which is expected due to higher sensitivity (i.e., 10-fold higher EF) of the former. MPs with Hex dye (with S2 or SC6 linker) and Cy5 dye (with S2 linker) also show excellent SERS spectra on our substrates (Figure S-3 in the Supporting Information).

The target detection limit is a critically important parameter for any MP assay. For our RSV assay, the detection limit is affected by a number of factors, including stability (e.g., fluorescence bleaching) of the dye, surface coverage of the MP covalently bound to the SERS substrate, the presence of physisorbed, rather than covalently bound MPs on the SERS substrate, the nature of the thiol linker used, and optimization of the metal particle size distribution and surface morphology, among others. For the nonoptimized system described here, the detection limit of the dye currently represents the major factor

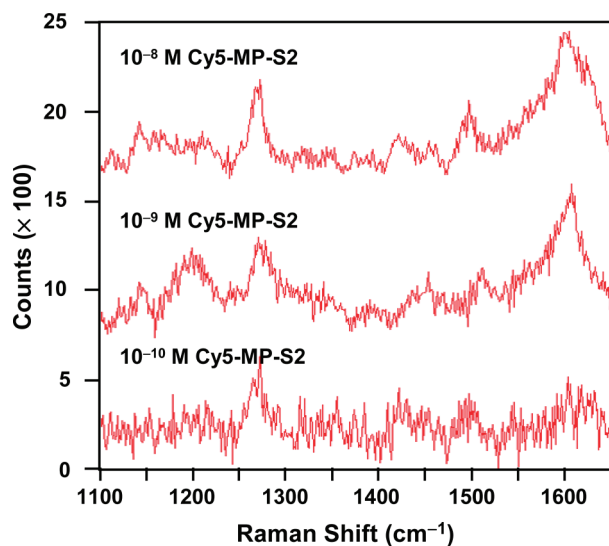


Figure 7. SERS spectra of Cy5-MP (with S2 linker) collected under three concentrations on Au metallized nanoPPX substrate. The detection limit for this probe is 10⁻¹⁰ M.

affecting the sensitivity and detection limit for the RSV target and therefore functions as an effective proxy for the RSV detection limit and assay sensitivity. For example, for our experiments, the number of RNA molecules in a 1 nM solution is approximately 1000 molecules per μm² area assuming a 1 μL analyte solution containing 6 × 10⁸ molecules (=1 μL × 10⁻⁹ M × 6.02 × 10²³), a 1 μm laser spot size (=0.61 λ/N.A = 0.61 × 632 nm/0.4), and a 0.76 mm² surface coverage of the drop (e.g., the contact angle of water is approximately 90° on Ag). Only a small percentage of the 1000 molecules are located at the hot spots to provide the maximum Raman enhancement on the surface. Therefore, we examined the response of our MP bound to the Au-nanoPPX SERS substrate (scheme C) as a function of the level of Cy5-MP-S2 probe present in Figure 7. The SERS spectrum in Figure 7 displays fingerprint vibration modes of the Cy5 dye and low detection limit (~10⁻¹⁰ M), consistent with previously reported, analogous

SERS studies on FBT,¹⁴ creatinine,⁴⁰ *Escherichia coli*,¹⁴ and RSV particles.⁴¹ We also note that the substrates have high spatial uniformity and reproducibility (i.e., <10% variation). Reproducibility of the SERS spectra is reported in the Supporting Information (Figure S-4) at a higher concentration of the analyte.

4. Conclusions

In summary, we have demonstrated the detection of RSV gene using SERS substrates fabricated by metallizing nanoPPX film via electroless (i.e., scheme B) or vapor deposition (i.e., scheme C) methods. The advantage of these substrates is that no template or lithography is involved, thus providing a simple, inexpensive, and quick method to achieve a sensitive and reproducible SERS substrate. Electroless methods provide a significant advantage in that they allow selective metal deposition on catalyst sites, unlike vapor phase deposition where metal growth is largely unregulated. Using electroless methods, metal particle size and particle–particle separation can be tuned by controlling the size and surface coverage of the Pd colloid used to catalyze the surface, thereby permitting EF optimization of each SERS substrate. In addition, use of an aromatic ligand (e.g., pyridine) provides a means to anchor the metal particle on the nanoPPX surface, resulting in improved stability and robustness of the substrate. Moreover, the ligand functionalization approach is particularly effective in mimicking the three-dimensional nanoarchitecture of the underlying nanoPPX template, thereby inducing additional Raman enhancement and allowing detection of large biomolecules.^{9,12,42} Given these advantages, we have successfully employed our substrates, specifically those prepared via schemes B and C from Figure 1, for SERS-based detection of RSV gene sequence. The use of MPs combined with SERS for oligonucleotide detection is an enabling technology, and rapid data analyses can be performed to determine specific genes. We are exploring methods to improve the SERS performance of our substrates, specifically for biological applications, by means of engineering the substrate morphology at the polymer template deposition and/or metal deposition stages.

Acknowledgment. The work was supported by the Pennsylvania State University, International Center for Materials Research at the University of California, Santa Barbara, and the Office of Naval Research under the Naval Research Laboratory Core 6.1 Research Program and the Young Investigator Program (M.C.D.). We gratefully acknowledge Professor David L. Allara for allowing access to the Raman equipment in his laboratory. We thank Dr. Hui Wang for assisting in SERS data collection and Dr. Josh Maier for the TEM images.

Supporting Information Available: AFM images of scheme B substrates; SERS spectra of Cy5-SC6 hybridized with genomic RSV RNA; SERS spectra of Cy5-S2, Hex-S2, and Hex-SC6 in nonhybridized configuration, and SERS spectra of S2-Cy5MP showing reproducibility data. This material is available free of charge via the Internet at <http://pubs.acs.org>.

References and Notes

- (1) Fleischm, M.; Hendra, P. J.; McQuilla, A. J. *Chem. Phys. Lett.* **1974**, *26*, 163–166.
- (2) Jeanmaire, D. L.; Vanduyne, R. P. *J. Electroanal. Chem.* **1977**, *84*, 1–20.

- (3) Albrecht, M. G.; Creighton, J. A. *J. Am. Chem. Soc.* **1977**, *99*, 5215–5217.
- (4) Orendorff, C. J.; Gole, A.; Sau, T. K.; Murphy, C. J. *Anal. Chem.* **2005**, *77*, 3261–3266.
- (5) Tian, Z. Q.; Yang, Z. L.; Ren, B.; Li, J. F.; Zhang, Y.; Lin, X. F.; Hu, J. W.; Wu, D. Y. *Faraday Discuss.* **2006**, *132*, 159–170.
- (6) Wang, T.; Hu, X. G.; Dong, S. J. *J. Phys. Chem. B* **2006**, *110*, 16930–16936.
- (7) Sztainbuch, I. W. *J. Chem. Phys.* **2006**, *125*, 124707.
- (8) Grabar, K. C.; Smith, P. C.; Musick, M. D.; Davis, J. A.; Walter, D. G.; Jackson, M. A.; Guthrie, A. P.; Natan, M. J. *J. Am. Chem. Soc.* **1996**, *118*, 1148–1153.
- (9) Kahraman, M.; Aydin, O.; Culha, M. *ChemPhysChem* **2009**, *10*, 537–542.
- (10) Aroca, R. F.; Goulet, P. J. G.; dos Santos, D. S.; Alvarez-Puebla, R. A.; Oliveira, O. N. *Anal. Chem.* **2005**, *77*, 378–382.
- (11) Goulet, P. J. G.; dos Santos, D. S.; Alvarez-Puebla, R. A.; Oliveira, O. N.; Aroca, R. F. *Langmuir* **2005**, *21*, 5576–5581.
- (12) Wang, T.; Hu, X. G.; Wang, J. L.; Dong, S. J. *Talanta* **2008**, *75*, 455–460.
- (13) Deng, S.; Fan, H. M.; Zhang, X.; Loh, K. P.; Cheng, C. L.; Sow, C. H.; Foo, Y. L. *Nanotechnology* **2009**, *20*, 175705.
- (14) Kao, P.; Malvadkar, N. A.; Cetinkaya, M.; Wang, H.; Allara, D. L.; Demirel, M. C. *Adv. Mater.* **2008**, *20*, 3562–3565.
- (15) Ko, H.; Chang, S.; Tsukruk, V. V. *ACS Nano* **2009**, *3*, 181–188.
- (16) Amezcuca-Correa, A.; Yang, J.; Finlayson, C. E.; Peacock, A. C.; Hayes, J. R.; Sazio, P. J. A.; Baumberg, J. J.; Howdle, S. M. *Adv. Funct. Mater.* **2007**, *17*, 2024–2030.
- (17) Cetinkaya, M.; Malvadkar, N.; Demirel, M. C. *J. Polym. Sci., Polym. Phys.* **2008**, *46*, 640–648.
- (18) Cetinkaya, A.; Boduroglu, S.; Demirel, M. C. *Polymer* **2007**, *48*, 4130–4134.
- (19) Demirel, M. C. *Colloids Surf., A* **2008**, *321*, 121–124.
- (20) Ma, D. I.; Shirey, L.; McCarthy, D.; Thompson, A.; Qadri, S. B.; Dressick, W. J.; Chen, M.-S.; Calvert, J. M.; Kapur, R.; Brandow, S. L. *Chem. Mater.* **2002**, *14*, 4586–4594.
- (21) Dobisz, E. A.; Bass, R.; Brandow, S. L.; Chen, M.-S.; Dressick, W. J. *Appl. Phys. Lett.* **2003**, *82*, 478–480.
- (22) Demirel, M. C.; Cetinkaya, M.; Singh, A.; Dressick, W. J. *Adv. Mater.* **2007**, *19*, 4495–4499.
- (23) Malvadkar, N.; Park, S.; Urquidi-MacDonald, M.; Wang, H.; Demirel, M. C. *J. Power Sources* **2008**, *182*, 323–328.
- (24) Gorham, W. F. *J. Polym. Sci. A-1* **1966**, *4*, 3027–3039.
- (25) Dressick, W. J.; Kondracki, L. M.; Chen, M.-S.; Brandow, S. L.; Matijević, E.; Calvert, J. M. *Colloids Surf., A* **1996**, *108*, 101–111.
- (26) Malvadkar, N.; Dressick, W. J.; Demirel, M. C. *J. Mater. Chem.* **2009**, *19*, 4796–4804.
- (27) Malvadkar, N.; Sekeroglu, K.; Dressick, W. J.; Demirel, M. C. *Langmuir* **2010**, *26*, 4382–4391.
- (28) Zabetakis, D.; Dressick, W. J. *ACS Appl. Mater. Interfaces* **2009**, *1*, 4–25.
- (29) Dressick, W. J.; Dulcey, C. S.; Georger, J. H.; Calabrese, G. S.; Calvert, J. M. *J. Electrochem. Soc.* **1994**, *141*, 210–220.
- (30) Brandow, S. L.; Dressick, W. J.; Marrian, C. R. K.; Chow, G. M.; Calvert, J. M. *J. Electrochem. Soc.* **1995**, *142*, 2233–2243.
- (31) Dixon, M. C.; Daniel, T. A.; Hieda, M.; Smilgies, D. M.; Chan, M. H. W.; Allara, D. L. *Langmuir* **2007**, *23*, 2414–2422.
- (32) Szafranski, C. A.; Tanner, W.; Laibinis, P. E.; Garrell, R. L. *Langmuir* **1998**, *14*, 3580–3589.
- (33) So, E.; Demirel, M. C.; Wahl, K. J. *J. Phys. D: Appl. Phys.* **2010**, *43*, 045403.
- (34) Boduroglu, S.; Cetinkaya, M.; Dressick, W. J.; Singh, A.; Demirel, M. C. *Langmuir* **2007**, *23*, 11391–11395.
- (35) Emery, S. R.; Haskins, W. E.; Nie, S. M. *J. Am. Chem. Soc.* **1998**, *120*, 8009–8010.
- (36) Ung, T.; Liz-Marzan, L. M.; Mulvaney, P. J. *J. Phys. Chem. B* **2001**, *105*, 3441–3452.
- (37) Tyagi, S.; Kramer, F. R. *Nat. Biotechnol.* **1996**, *14*, 303–308.
- (38) Strohsahl, C. M.; Miller, B. L.; Krauss, T. D. *Nat. Protoc.* **2007**, *2*, 2105–2110.
- (39) Faulds, K.; Fruk, L.; Robson, D. C.; Thompson, D. G.; Enright, A.; Smith, W. E.; Graham, D. *Faraday Discuss.* **2006**, *132*, 261–268.
- (40) Wang, H.; Malvadkar, N.; Koytek, S.; Bylander, J.; Reeves, W. B.; Demirel, M. C. *J. Biomed. Opt.* **2010**, *15*, 027004.
- (41) Demirel, M. C.; Kao, P.; Malvadkar, N.; Wang, H.; Gong, X.; Poss, M.; Allara, D. L. *Biointerphases* **2009**, *4*, 35–41.
- (42) Lu, L. H.; Randjelovic, I.; Capek, R.; Gaponik, N.; Yang, J. H.; Zhang, H. J.; Eychmuller, A. *Chem. Mater.* **2005**, *17*, 5731–5736.